Windmilling Characteristics of Centrifugal-Flow Turbojets

Yoo Il Su*
School of Mechanical Engineering, Korea Advanced Institute of Science and Technology, Guseong-Dong, Yuseong-Gu, Daejon 305-701, Korea
Song Seung Jin
School of Mechanical and Aerospace Engineering, Seoul National University, San 56-1, Sillim-Dong, Gwanak-Gu, Seoul 151-742, Korea
Lim Jin Shik
Agency for Defense Development, P.O. Box 35, Yuseong-Gu, Daejon, Korea

A new nondimensional method for predicting the windmilling performance of centrifugal -flow turbojet engines in flight has been developed. The method incorporates loss correlations to estimate the performance of major engine components. Given basic engine geometry, flight Mach number, and ambient conditions, this method predicts transient and steady-state windmilling performance. Thus, this method can be used during the preliminary design stage when detailed hardware geometry and component performance data are not yet available. A nondimensional time parameter is newly defined, and using this parameter, the transient performance of different types of turbojets (e.g. centrifugal vs. axial) is compared. In addition, the predictions' sensitivity to loss correlations, slip factors, and inlet ambient temperatures are analyzed.

Key Words : Turbouet Engine, Windmilling, Transient Performance, Loss Analysis, Non-Dimensional Parameter

Nomenclature

A : Area
a : Acoustic velocity
b : Blade height
C : Absolute velocity
C_f : Friction factor
DF : Diffusion factor
d : Diameter
g_c : Constant in the force equation
h : Enthalpy
I : Moment of inertia
i : Incidence angle
K_f : Torque coefficient
L : Length
M : Mach number
M_u : Tangential Mach number at tip
$\dot{m}$: Mass flow rate
N : Rotational speed
P : Total pressure
ΔP_B : Total pressure loss at combustor
Q : Torque
R : Gas constant
r : Radius
Re : Reynolds number
s : Entropy
T : Temperature
t : Time
U : Blade rotational speed
W : Relative velocity
Z : Blade number
Δ : Finite change
α : Absolute flow angle
β : Relative flow angle
δ : Nondimensional excess torque

* Corresponding Author,
E-mail : isyoo@kaist.ac.kr
TEL : +82-42-869-3054; **FAX** : +82-42-869-0000
School of Mechanical Engineering, Korea Advanced Institute of Science and Technology, Guseong-Dong, Yuseong-Gu, Daejon 305-701, Korea. (Manuscript **Received** July 24, 2003; **Revised** August 16, 2004)

ε : Blade tip clearance
γ : Specific heat ratio
η : Efficiency
κ : Kinetic energy loss coefficient
μ : Slip factor
ν : Kinematic viscosity
θ : Nondimensional mass flow rate
ρ : Density
τ : Nondimensional time
ξ : Loss coefficient
ψ : Blade loading coefficient

Subscripts

a : Ambient condition
b : Blade angle
bl : Blade loading
cl : Clearance
cr : Critical
des : Design condition
df : Disk friction
HB : Hydraulic mean
h : Hub
i : Inlet duct
in : Stage inlet
inc : Incidence
L : Normal component to the optimum flow direction
LJ : Normal component to the meridional flow direction
m : Meridional, mechanical
mix : Mixed conditional
n : Step
noz : Exhaust nozzle
opt : Optimum
out : Stage exit
r : Rotor
rc : Recirculation
s : Stator
sf : Skin friction
std : Standard consition
t : Tip
vd : Vaned diffuser
vld : Vaneless diffuser
w : Circumferential direction
0 : Stagnation state, upstream of compressor
1 : Impeller inlet
2 : Impeller exit
$2D$: Vaneless diffuser inlet
$2vl$: Vaneless diffuser exit
3 : Turbine rotor inlet
4 : Turbine rotor exit

Superscripts

$'$: Relative condition

1. Introduction

Several methods are used to restart turbojet engines in flight. Typical methods include the use of auxiliary power units, cartridges, or windmilling. Among these, the windmilling method is probably the simplest and requires no special accessory equipment. However, it takes relatively long time due to slow acceleration. Windmilling can occur under different circumstances. When a turbojet engine in flight experiences an engine flameout, its rotational speed drops rapidly until a steady windmilling state is established. On the other hand, when a turbojet engine is suddenly exposed to ram air, rotor begins self-rotation and accelerates to a steady windmilling state. Prediction of such windmilling characteristics is important in determining engine starting system requirements. Yet open literature on starting turbojet engines in flight is scarce, and, therefore, predicting windmilling performance is difficult.

Three different approaches can be used for windmilling analysis of turbojet engines. One is to generate correlations from in-flight experimental windmilling data for different engines. It has the advantage of being accurate, but it is expensive and the results cannot be generalized. Another is to use performance maps for each engine component which covers the low speed range. Together with pressure loss data for other engine parts, a system performance analysis can be done. This method can be done without flight tests. However, it is difficult and expensive to obtain such off-design data. Third approach is to utilize the available cascade data to estimate compressor and turbine loss parameters. The first two methods require expensive off-design testing, but the latter uses existing literature. However, its accuracy needs to be verified.

Choi et al.(1996) predicted the windmilling performance of axial turbojet engines by using cascade data to predict compressor and turbine losses. The predicted results were in good agreement with the available experimental data as shown in Figs. 1 and 2. Also, a similar agreement for turbofan engines was obtained by Kang et al. (1997). Thus, the method based on cascade data can accurately predict the windmilling performance of axial turbojet engines. However, a similar analysis for centrifugal engines has not yet been carried out.

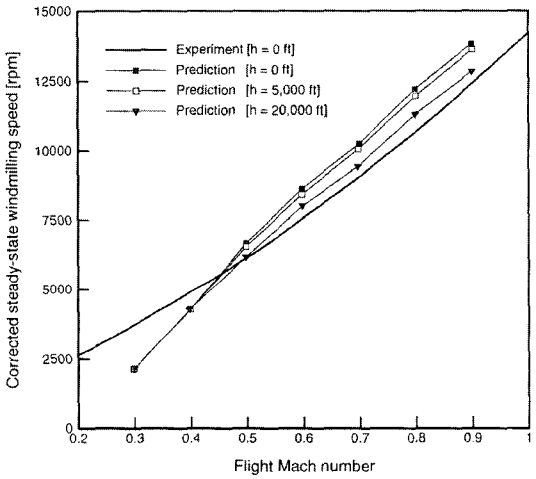

Fig. 1 Effects of flight Mach number and altitude on steady state windmilling speed (Choi et al., 1996)

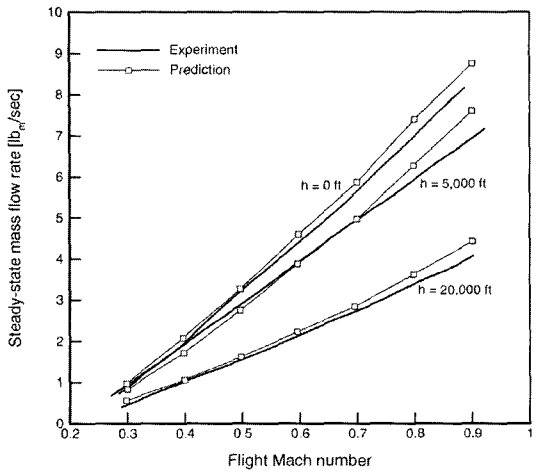

Fig. 2 Effects of flight Mach number and altitude on engine mass flow rate under steady state windmilling condition (Choi et al., 1996)

The objective of present study is to develop a practical method to investigate windmilling in a centrifugal-flow turbojet engine. The paper presents a new nondimensional analysis. Under various flight Mach number and ambient conditions, transient and steady-state windmilling speeds are predicted. Component losses are estimated from two-dimensional correlations, and their effects are predicted.

2. Definition of Parameters

The benefits of dimensional analysis are well known. First, the number of variables can be reduced, and, thus, save time and expense related to experiments. Second, non-dimensional parameters enable generalization and concise presentation of data. Thus, designers can assess not only the performance of a given machine at different operating conditions but also the performance of other geometrically similar machines and scale existing designs to different sizes. However, such parameters have not yet been defined for windmilling analysis. Therefore, the nondimensional parameters relevant to windmilling analysis are defined below.

The nondimensional impeller tip speed is obtained by normalizing the impeller tip speed by the speed of sound based on the inlet stagnation temperature.

$$M_u=\frac{U_2}{a_{01}}=\frac{2\pi r_2 N}{60\sqrt{\gamma R T_{01}}} \tag{1}$$

The non-dimensional mass flow parameter is defined to be the ratio of the actual mass flow rate to the maximum possible mass flow rate through an orifice of radius r_2:

$$\theta=\frac{\dot{m}}{\rho_{01}a_{01}\pi r_2^2}=\frac{\dot{m}\sqrt{RT_{01}/\gamma}}{P_{01}\pi r_2^2} \tag{2}$$

The ideal total enthalpy changes which occur through compressors and turbines are expressed by blade loading coefficients. The actual blade loading coefficient values differ from the ideal ones due to the exit flow deviation. Therefore, slip factor μ is adopted to calculate the actual com-

pressor blade loading coefficient. For the turbine, the deviation effects are not as severe. Therefore, ideal blade loading coefficients values are used for the turbine.

$$\psi_1 = \mu\psi_{1\,ideal}$$

$$\psi_{1\,ideal} = \frac{1}{1-\tan\beta_{2b}/\tan\alpha_2} \quad \text{(zero pre-swirl)} \quad : \text{compressor} \quad (3)$$

$$\psi_3 = \psi_{3\,ideal} = \left(\frac{r_3}{r_2}\right)^2\left(\frac{1}{1-\tan\beta_3/\tan\alpha_{3b}} - \frac{1}{1-\tan\beta_{4b}/\tan\alpha_4}\right) \quad : \text{turbine} \quad (4)$$

Excess torque is the difference between the turbine torque and the compressor torque. Non-dimensional ideal excess torque δ is defined as follows,

$$\delta = \frac{\Delta Q}{a_{01}^2\rho_{01}\pi r_2^3} = \theta M_u \Delta\psi \quad (5)$$

where $\Delta\psi$ is the difference between the actual turbine enthalpy change and the actual compressor enthalpy change.

The actual excess torque is reduced by various mechanical and aerodynamic losses, and correlation are need to predict these losses. The time required for rotor acceleration is calculated from the following equation.

$$\Delta t = \frac{2\pi I(N_{n+1}-N_n)}{60\Delta Q} \quad (6)$$

The t is then non-dimensionalized as shown in Eq. (7). The denominator is the characteristic time determined from the engine geometry and ambient inlet conditions.

$$\tau = \frac{t}{\left(\frac{I}{a_{01}\rho_{01}\pi r_2^4}\right)} = \frac{1}{\theta\Delta\psi} = \frac{M_u}{\delta} \quad (7)$$

3. Calculation Procedure

The calculation procedure is composed of two iteration loops as shown in Fig. 3. The inner loop is to satisfy the continuity condition among different engine components. The outer loop calculates excess torque and updates engine speed

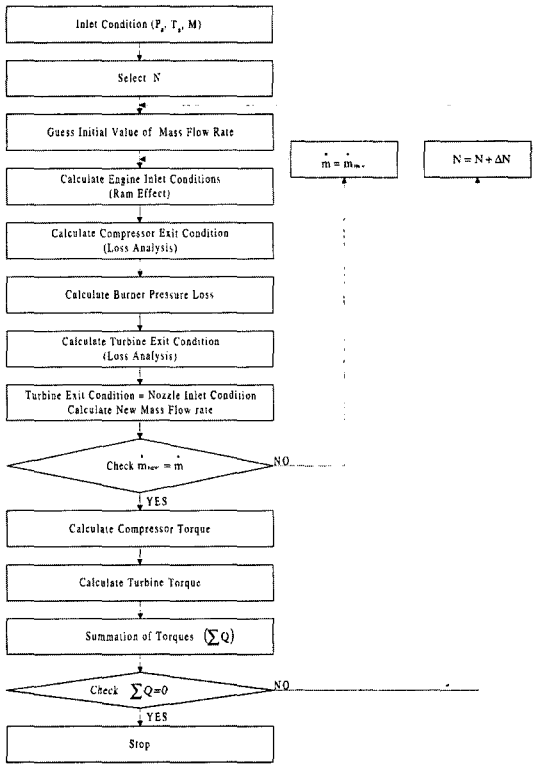

Fig. 3 Calculation process flow chart

(rpm) until steady state is reached. Detailed explanations are given in Appendix 1.

4. Model Predictions and Sensitivity Analysis

4.1 Test turbojet specification

A turbojet engine, composed of a single-stage centrifugal compressor, a combustor, and a single-stage axial turbine, is used in the present study.

Table 1 Test engine specification

Engine type	Centrifugal-flow turbojet engine
Engine speed	42,000 rpm
Mass flow rate	6.90 kg/sec
Total pressure ratio	3.80
Adiabatic efficiency of the compressor	80%
Exit tip radius of the compressor	0.1388 m
Adiabatic efficiency of the turbine	84%
Moment of inertia	0.06 kgm^2

The engine's design point specifications are presented in Table 1.

4.2 Ideal prediction

In an ideal case without losses, the slip factor and impeller efficiency are equal to one. Also, the mass flow rate is the largest, and the excess torque is the biggest. Therefore, predictions for the ideal case are presented as a reference.

As shown in Fig. 4, the mass flow rate decreases during the starting mode. The mass flow rate is proportional to the total pressure and inversely proportional to the total temperature at the inlet of the exhaust nozzle. During the transient windmilling phase, the compressor goes through the turbine mode, frictional duct mode, and finally compressor mode as its rotational speed increases. At the beginning, due to its low rotational speed, the compressor doesn't impart energy but absorbs energy from the air flow. Thus, the total pressure at compressor exit is lower than that at the inlet, and the total pressure at the nozzle inlet is reduced, decreasing the mass flow rate decreases from its initial value. As the engine is further accelerated, the compressor's work goes to zero. Thus, the compressor behaves like a frictional duct, and the mass flow rate reaches its minimum value. At higher rotating speeds, the compressor loading becomes positive, and the exit total pressure increases, and thus, the mass flow rate increases. The variation of rotating speed versus time is shown in Fig. 5. Unlike the mass flow rate, the rotational speed increases continuously.

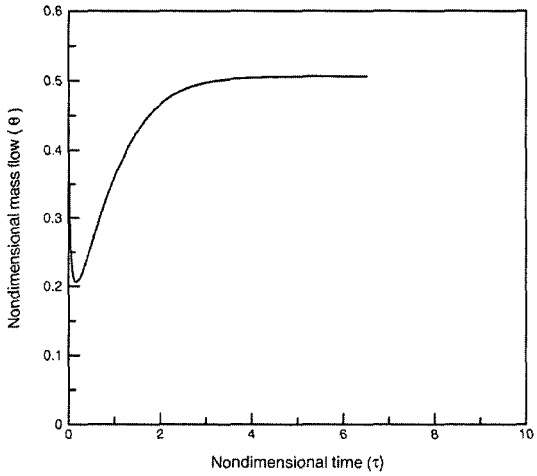

Fig. 4 Dependence of θ on τ in the ideal case

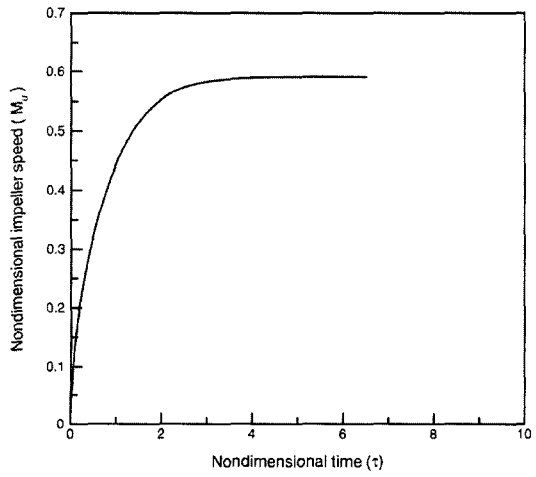

Fig. 5 Dependence of M_u on τ in the ideal case

4.3 Sensitivity analysis

4.3.1 Impeller loss correlation

Losses in impeller arise from various origins. Common loss generating mechanisms include those due to incidence, skin friction, blade loading, impeller shroud clearance, and mixing. It has been shown that loss formulations based on these mechanisms provide a realistic representation of the actual situation.

Present study has tested many impeller loss models previously reported in the open literature (Augier, 1990 and 1995; Conrad et al., 1980; Coppage et al. 1956; Daily and Nece, 1960; Galvas, 1973; Jansen, 1967; Krylov and Spunde, 1991; Rodgers, 1978; Whitfield and Baines, 1990; Whitfield and Wallace, 1975). Various empirical loss models for each loss mechanism were collected, categorized, and compared. Set I is the combination of loss models which predict the smallest entropy creation. Set III is the combination of loss models which predict the largest entropy creation. And, Set II is the combination of loss models which predict entropy creation between Set I and Set III. Table 2 lists each loss set. For all three sets, same loss models have been

Table 2 Three sets of loss correlations

Loss mechanisms		Set I	Set II	Set III
Types of impeller losses	Incidence	Aungier (1995)	Galvas (1973)	Conrad (1980)
	Skin friction	Coppage (1956)	Jansen (1967)	Rodgers (1978)
	Blade loading	Rodgers (1978)	Coppage (1956)	Coppage (1956)
	Clearance	Aungier (1995)	Jansen (1967)	Krylov (1991)
	Mixing	Whitfield (1975)	Whitfield (1975)	Whitfield (1975)

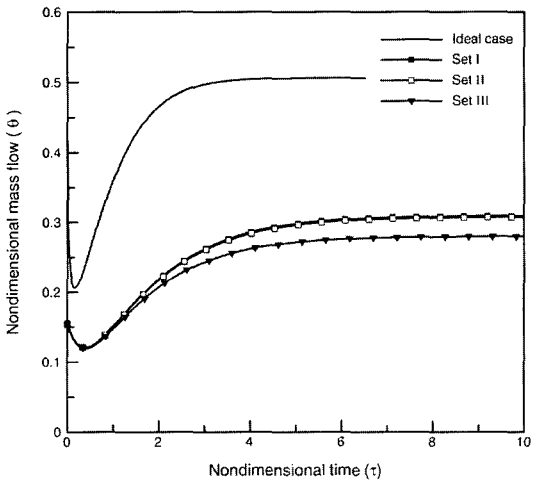

Fig. 6 Dependence of θ on τ according to the loss sets

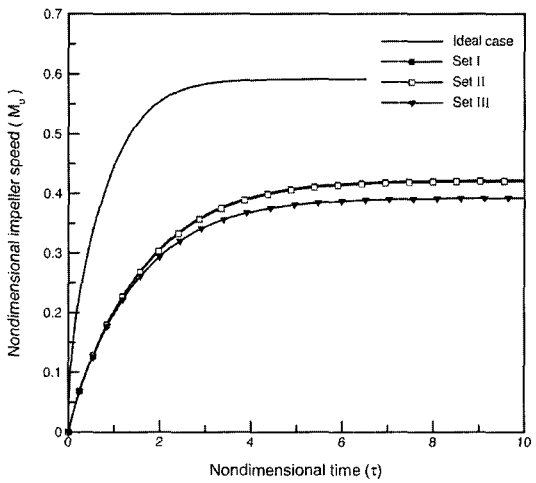

Fig. 7 Dependence of M_u on τ according to the loss sets

applied to estimate the diffuser loss, external loss, and axial turbine losses. Detailed loss models are given in Appendix 2.

Figure 6 shows plots of the nondimensional mass flow rate versus the nondimensional time. Along the operation line, the non-dimensional mass flow rate is directly proportional to compressor pressure. The compressor's swallowing capacity increases with rotational speed. Therefore, mass flow rate increases with pressure ratio. Increased entropy creation at the same ram pressure decreases pressure ratio. Thus, for Set III, the mass flow rate is the smallest compared to other cases (Fig. 6). In Eq. (3), ψ_1 is proportional to the slip factor and α_2. In turn, α_2 is proportional to slip factor and inversely proportional to mass flow rate. Thus, ψ_1 is affected by the slip factor and mass flow rate. However, ψ_3, Eq. (4), is more sensitive to mass flow rate than slip factor. Furthermore, the mass flow rate is affected by pressure ratio that is proportional to the impeller efficiency. Since the same slip factor is used for all three loss sets in Table 2, only the compressor efficiency varies. With higher impeller efficiency, less entropy is created, and mass flow rate is increased. The increase in mass flow rate increases the turbine blade loading but decreases the compressor blade loading. Therefore, the excess blade loading is increased, and the steady-state windmilling speed is higher. Also, the time to reach steady-state windmilling speed is shorter as acceleration increases (Fig. 7).

4.3.2 Slip factor

In the present section, the sensitivity of performance estimation vs. slip factor is presented. Slip factor estimation is essential to predict the performance of centrifugal compressors. The slip factor is arbitrarily assumed to vary from 0.8 to 1.0. Wiesner's correlation (1967) results in a

value of 0.91. The loss correlation Set II is applied equally to each case. Therefore, the compressor efficiency remains constant, and only the effect of slip factor is compared at the condition of standard sea level and flight Mach number 0.5.

As the slip factor increases, the compressor blade loading increases. However, the turbine blade loading increases less than the compressor blade loading, and the steady state windmilling speed decreases as shown in Fig. 9. However, the transient windmilling performance hardly varies because the excess torque δ, which is determined by the excess blade loading $\Delta\psi$ and the mass flow rate θ (Eq. (5)), stays approximately constant.

4.3.3 Inlet conditions

A parametric study was carried out to examine the sensitivity of model predictions to variations in inlet conditions. The effect of ambient temperature was investigated by varying the standard ambient temperature at 20,000 ft by ±5%. The effect of inlet flow angle was investigated by

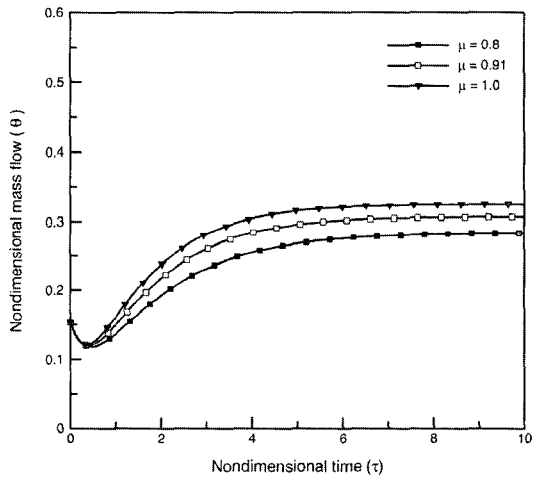

Fig. 8 Dependence of θ on τ according to the slip factors

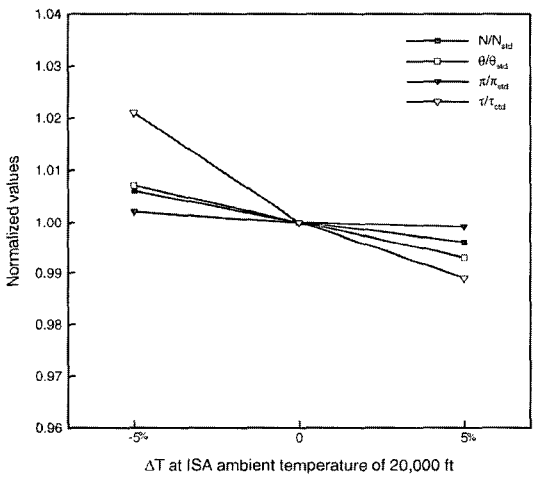

Fig. 10 The effect of ambient temperature variation [M=0.5, ISA at 20,000 ft]

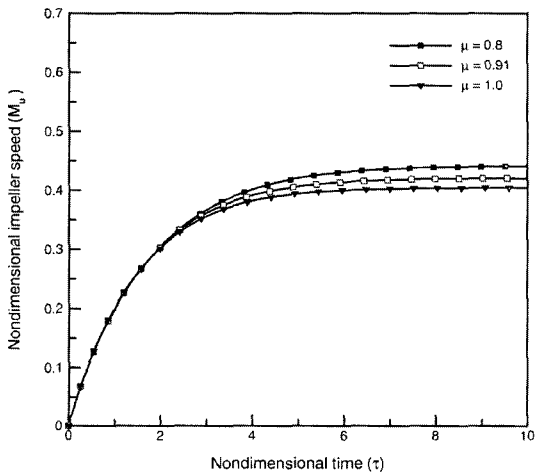

Fig. 9 Dependence of M_u on τ according to the slip factors

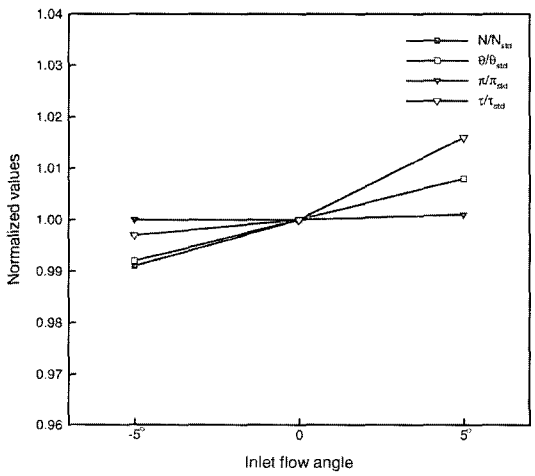

Fig. 11 The effect of inlet flow angle variation [M=0.5, ISA at 20,000 ft]

Table 3 Design specifications of centrifugal and axial turbojet engines

Engine type	Centrifugal turbojet	Axial turbojet
Engine speed	42,000 rpm	29,500 rpm
Mass flow rate	6.90 kg/sec	6.25 kg/sec
Total pressure ratio	3.80	3.95
Adiabatic compressor efficiency	80%	75%
Exit tip radius of the compressor	0. 1388 m	0. 1053 m
Adiabatic turbine efficiency	84%	82%
Moment of inertia	0.06 kgm^2	0.078 kgm^2

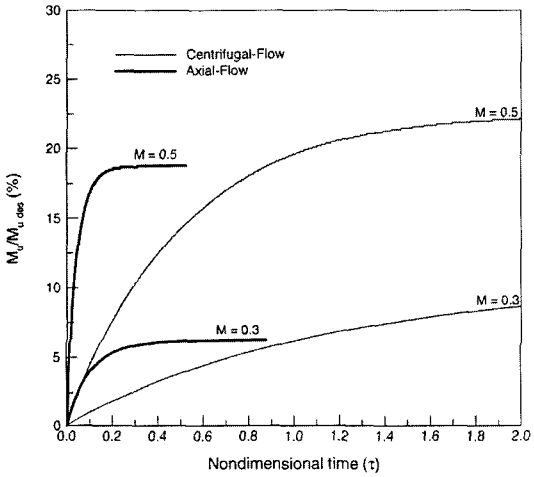

Fig. 12 Comparison of windmilling speed between centrifugal and axial turbojets

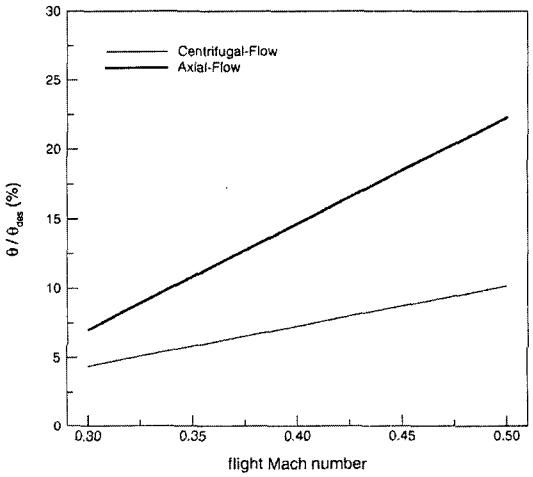

Fig. 13 Comparison of mass flow rate between centrifugal and axial turbojets

varying the inlet angle by $\pm 5°$ from the axial direction. In this study, the loss model Set II and Wiesner's correlation were used. Figs. 10 and 11 show the results of sensitivity analysis. The effects of the ambient condition and inlet flow angle are negligibly small for the ranges tested.

4.4 Axial vs. centrifugal turbojet

Next, the windmilling performance of a centrifugal turbojet engine is compared with that of an axial turbojet engine (TRI-60). The design performance for both engines are listed in Table 3.

The windmilling performance of both centrifugal and axial turbojet engines are plotted versus flight Mach number (Fig. 12). Here, the windmilling performance of centrifugal turbojet engine is estimated by using the loss correlation Set II in Table 2 and the results are compared with those for an axial turbojet engine given in Choi et al. (1996). The horizontal axis denotes the nondimensional time and the vertical axis is the ratio of $M_u/M_{u\,des}$. As shown in Fig. 12, the steady-state windmilling speed of the centrifugal turbojet is higher than that of the axial turbojet at all flight Mach numbers.

When the steady state, nondimensional time is less than one, it means that the steady state windmilling can be accomplished prior to the characteristic time. The non-dimensional time to reach steady state windmilling speed of axial turbojet is less than 0.4, but that of centrifugal turbojet is greater than 2 at all flight Mach numbers. This delay occurs mainly because the air flow through the centrifugal engine is less than that through the axial engine (Fig. 13).

5. Conclusions

(1) A nondimensional prediction method has been developed and used to analyze both transient and steady state windmilling performance of a centrifugal-flow turbojet engine.

(2) The sensitivity of performance predictions to various loss correlations was investigated. Relative to the ideal (no loss) case, the time to reach steady state almost doubled, and the steady state windmilling speed decreased by as much as 1/3.

(3) Transient characterists were less sensitive to the slip factor variation. Compared to the no slip case, the time to reach steady state and the steady state windmilling speed both increased about 10%.

(4) Ambient condition and inlet flow perturbations did not significantly affect predictions.

(5) A centrifugal-flow turbojet takes longer to reach steady state than an axial-flow engine due to the reduced mass flow rate in the centrifugal-flow engine.

Acknowledgment

This work was supported by the Agency for Defense Development, the Micro Thermal System Research Center of the Korea Science and Engineering Foundation and Seoul National University Hyundai Fund. The authors thank Professor Yong-Shik Hong and Mr. Min-Su Choi for their helpful comments.

References

Aungier, R. H., 1990, "Aerodynamic Performance Analysis of Vaned Diffusers," *Fluid Machinery Components, ASME FED*, Vol. 101, pp. 27~44.

Aungier, R. H., 1995, "Mean Streamline Aerodynamic Performance Analysis of Centrifugal Compressors," *ASME Journal of Turbomachinery*, Vol. 117, pp. 360~366.

Choi, M. S., Lim, J. S. and Hong, Y. S., 1996, "A Practical Method for Predicting the Windmilling Characteristics of Simple Turbo Jet Engines," *ASME TURBO ASIA '96*, Indonesia, Paper No. 96-TA-60.

Conrad, O., Raif, K. and Wessels, M., 1980, "The Calculation of Performance Maps for Centrifugal Compressors with Vane-Island Diffusers," *ASME 25th Annual International Gas Turbine Conference and 22th Annual Fluids Engineering Conference*, Louisiana, pp. 135~147.

Coppage, J. E., Dallenbach, F., Eichenberger, J. P., Hlavak, G. E., Kmoernschild, E. M. and Vanke, N., 1956, "Study of Supersonic Radial Compressors for Refrigeration and Pressurization Systems," WADC Report 55-257.

Daily, J. W. and Nece, R. E., 1960, "Chamber Dimension Effects on Induced Flow and Frictional Resistance of Enclosed Rotating Disks," *ASME Journal of Basic Engineering*, Vol. 82, pp. 217~232.

Galvas, M. R., 1973, "FORTRAN Program for Predicting Off-Design Performance of Centrifugal Compressors," NASA TN D-7487.

Jansen, W., 1967, "A Method for Calculating the Flow in a Centrifugal Impeller When Entropy Gradients Are Present," *Royal Society Conference on Internal Aerodynamics (Turbomachinery)*, pp. 133~146.

Kang, I. S., Choi, M. S., Lim, J. S. and Hong, Y. Y., 1997, "Analysis of Windmilling Charateristics for Twin-Spool Turbofan Engine," *ASME ASIA '97*, Singapore, Paper No. 97-AA-113.

Krylov, P. and Spunde, A., 1991, "About the Influence of the Clearance Between the Working Blades and Housing of a Radial Turbine on Its Exponent," *Izvestiya VUZ. Energetika*, No. 7.

Rodgers, C., 1978, "A Diffusion Factor Correlation for Centrifugal Impeller Stalling," ASME Paper 78-GT-61.

Whitfield, A. and Baines, N. C., 1990, *Design of Radial Turbomachinery*, Longman Scientific and Technical.

Whitfield, A. and Wallace, F. J., 1975, "Performance Prediction for Automotive Turbocharger Compressors," *Proc. Instn Mech. Engrs., Part A*, Vol. 189, pp. 557~565.

Wiesner, F. J., 1967, "A Review of Slip Factors for Centrifugal Impellers," *ASME Journal of Engineering for Power*, Vol. 89, pp. 558~572.

Appendix 1

1. Input variables
   assumed efficiency : η_i, η_m, ΔP_B
   geometric variables :
   r_1, r_2, r_3, r_4, β_{1b}, β_{2b}, β_{3b}, β_{4b}, Z, A_{noz}, I
   ambient and flight conditions : P_a, T_a, M

2. Calculation of ram effect

$$P_1=P_a\left[1+\eta_i\frac{\gamma-1}{2}M^2\right]^{1/(\gamma-1)}$$

$$T_1=T_a\left[1+\frac{\gamma-1}{2}M^2\right]$$

3. Assume initial rotating speed and mass flow rate

4. Calculate total entropy creation in compressor

$$\Delta S=\frac{\gamma R}{1-\gamma}\ln\left[1-(\gamma-1)\left(\frac{\sum\Delta h}{\gamma R T_2'}\right)\right]$$

$$\sum\Delta h=\Delta h_{inc}+\Delta c_{sf}+\Delta h_{bl}+\Delta h_{mix}+\Delta h_{cl}+\Delta h_{vld}+\Delta h_{vd}+\Delta h_{df}+\Delta h_{rc}$$

5. Calculate compressor exit conditions

$$P_2'=P_1'\left(\frac{T_2'}{T_1'}\right)^{\gamma/(\gamma-1)}e^{-\frac{\Delta S}{R}}$$

6. Calculate combustor exit stagnation pressure from ΔP_B

7. Calculate stagnation pressure loss in the turbine stator

$$\Delta P_s=\frac{\rho\Delta h_s}{144g_c},\quad \Delta h_s=\kappa_s\left(\frac{C_{in}^2+C_{out}^2}{2}\right)$$

8. Calculate stagnation pressure losses in the turbine rotor

$$\Delta P_r=\frac{\rho\Delta h_r}{144g_c}$$

$$\Delta h_r=\kappa_r\left(\frac{W_{in}^2+W_{out}^2}{2}\right)+\frac{C_{in}^2\{1-\cos^n(i-i_{opt})\}}{2}\quad\begin{cases}n=2(+\text{incidence})\\ n=3(-\text{incidence})\end{cases}$$

9. Calculate turbine exit conditions : P_4, T_4, ρ_4

10. Calculate a new mass flow rate, $\dot{m}_{new}$

If $\dot{m}_{new}$ is different from the assumed mass flow rate, $\dot{m}$, go back to Step 3 and assume a new mass flow rate

11. Calculate compressor torque and turbine torque

12. Calculate excess torque

If the excess torque is not equal to zero, add time increment to Eq. (6), and calculate rotating speed increment from Eq. (6), and then repeat all the steps with this new rotating speed beginning with Step 3.

Appendix 2

1. Incidence loss

Galvas (1973):

$$\Delta h_{inc}=\frac{W_L^2}{2}$$

$$W_L=W_1\sin|\beta_1-\beta_{1_{opt}}|$$

$$\beta_{1_{opt}}=\tan^{-1}\left(\frac{A_0}{A_1}\tan\beta_{1b}\right)$$

Conrad et al.(1980):

$$\Delta h_{inc}=\xi\frac{W_{LJ}^2}{2}$$

$$W_{LJ}=W_1\sin\beta_1-W_1\sin\beta_{1_{opt}}$$

2. Skin friction loss

Jansen (1967):

$$\Delta h_{sf}=4C_f\frac{L_{HB}\bar{W}^2}{2d_{HB}}$$

$$\bar{W}=\frac{C_{1t}+C_2+W_{1t}+2W_{1h}+3W_2}{8}$$

3. Blade loading loss

Coppage et al.(1956):

$$\Delta h_{bl}=0.005DF^2U_2^2$$

$$DF=\left(1+\frac{W_2}{W_{1t}}\right)+\frac{0.6(C_{w2}U_2-C_{w1}U_1)}{\left\{\frac{z_2}{\pi}\left(1-\frac{d_1}{d_2}\right)+2\left(\frac{d_1}{d_2}\right)\right\}U_2^2}\left(\frac{W_2}{W_{1t}}\right)$$

4. Clearance loss

Jansen(1967):

$$\Delta h_{cl}=0.6\frac{\varepsilon}{b_2}\sqrt{\frac{4\pi}{Z_2b_2}\frac{(\gamma_{1t}^2-\gamma_{1h}^2)C_{w2}^3C_{m1}}{(r_2-r_{1t})(1+\rho_2/\rho_1)}}$$

5. Mixing loss

Whitfield(1975):

$$\Delta h_{mix}=\left(\frac{A_{2_{wake}}}{A_{2_{jet}}}\right)^2\frac{C_{m2}^2}{2},\quad A_{2_{wake}}=A_2-A_{2_{jet}}$$

6. Vaneless diffuser loss
Coppage et al. (1956):

$$\Delta h_{vld}=C_f\frac{r_2C_2^2\{1-(r_2/r_{2vl})^{1.5}\}}{1.5b_2\cos\alpha_2}$$

7. Disk friction loss
Daily & Nece (1960):

$$\Delta h_{df}=K_f\frac{\bar{\rho}r_2^2U_2^3}{4\dot{m}}$$

$$K_f=\frac{2.67}{Re_{df}^{0.5}},\quad Re_{df}<3\times10^5$$

$$K_f=\frac{0.0622}{Re_{df}^{0.2}},\quad Re_{df}\geq3\times10^5$$

$$Re_{df}=\frac{U_2r_2}{\nu_2}$$

$$\bar{\rho}=\frac{\rho_1+\rho_2}{2}$$

8. Recirculation loss
Jansen (1967):

$$\Delta h_{rc}=0.02DF^2\sqrt{\tan\alpha_2}\,U_2^2$$

9. Slip factor
Wiesner (1967):

$$\mu=1-\frac{\sqrt{\cos\beta_{2b}}}{Z_2^{0.7}},\quad \frac{r_1}{r_2}<\left(\frac{r_1}{r_2}\right)_{cr}$$

$$\mu=1-\frac{\sqrt{\cos\beta_{2b}}}{Z_2^{0.7}}\left\{1-\frac{r_1/r_2-(r_1/r_2)_{cr}}{1-(r_1/r_2)_{cr}}\right\},\quad \frac{r_1}{r_2}>\left(\frac{r_1}{r_2}\right)$$

$$\left(\frac{r_1}{r_2}\right)_{cr}\approx e^{-0.18\frac{\cos\beta_{2b}}{Z_2}}$$